Numerical Simulation of Nugget Formation in Spot Welding

Mechanical Design & Analysis Corporation

Takaya Kobayashi and Yasuko Mihara

***Abstract**: This paper provides a finite element model to predict the nugget development during resistance spot welding of steel sheets. The model employs the coupled thermal-electrical-mechanical analysis capability of Abaqus. The contact area and the interface pressure distribution are determined from a thermal-mechanical coupling in the analysis. The knowledge of interface pressure allows for accurate prediction of interfacial heat and electrical resistance, which have a dominant role in Joule heat generation. Temperature-dependent material properties for the coupled analysis are used. The significant parameters in the spot-welding process are current magnitude and frequency, welding time, sheet material and thickness, geometry of electrodes, and electrode force. The methodology developed in this paper demonstrates the applicability of Abaqus to predict the shape and size of weld nuggets with variation of each process parameter using standard input options. Using this methodology assists in adjusting welding parameters so that costly experimental works can be avoided.*

***Keywords**: Spot welding, Coupled thermal-electrical-structural analysis*

1. Introduction

Spot welding is a process in which contacting metal surfaces are joined by the heat obtained from the resistance to electric current. Work-pieces are held together under the pressure exerted by electrodes. Typically, the sheets are in the 0.5 to 3 mm thickness range. The process uses two shaped copper alloy electrodes to concentrate the welding current into a small spot and simultaneously clamp the sheets together. Forcing a large current through the spot melts the metal and forms the weld. The attractive feature of spot welding is that a lot of energy can be delivered to the spot in a very short time, which permits the welding to occur without excessive heating of the remainder of the sheet. From the physical point of view, the simulation of such a process requires a high coupling level to account for the interactions between electrical and thermal phenomena coming from the Joule effect and the temperature dependence of the material properties. Moreover, contact conditions between sheets and electrodes need to be carefully considered. Abaqus (6.11), the general-purpose finite element code, was used for its powerful automatic mechanism for fully coupled thermal-electrical-structural analysis. The nugget sizes and formation process predicted by Abaqus agreed well with empirical facts. The welding conditions (current magnitude and electrode force) to produce proper nuggets were accurately estimated by the simulation.

2. Analysis model and loading conditions

Figure 1 shows the analysis model. The basic configuration of the model was cited from reference [2]. Two sheets of 1.6mm thick steel are superposed, and two copper alloy electrodes are simultaneously used to clamp the sheets together and to pass current through the sheets. The faying surfaces are not only mechanically contacted but also thermally and electrically contacted. Spot welding uses the electrical resistance on the interface to generate Joule heat so that the melting of steel sheets occurs in the intended portion with the appropriate size and shape, which is the so-called *nugget zone* of the weld. Therefore, the key issue in the analysis is the representation of the interface resistances depending on the contact conditions. Dome radius type electrodes with a diameter of 6mm and a radius of 40mm front face are assumed. Coupled analyses are performed on a quarter symmetric model, including about 4,000 solid elements. Element types Q3D8 and Q3D6 are available for the coupled thermal-electrical-structural analysis in Abaqus.

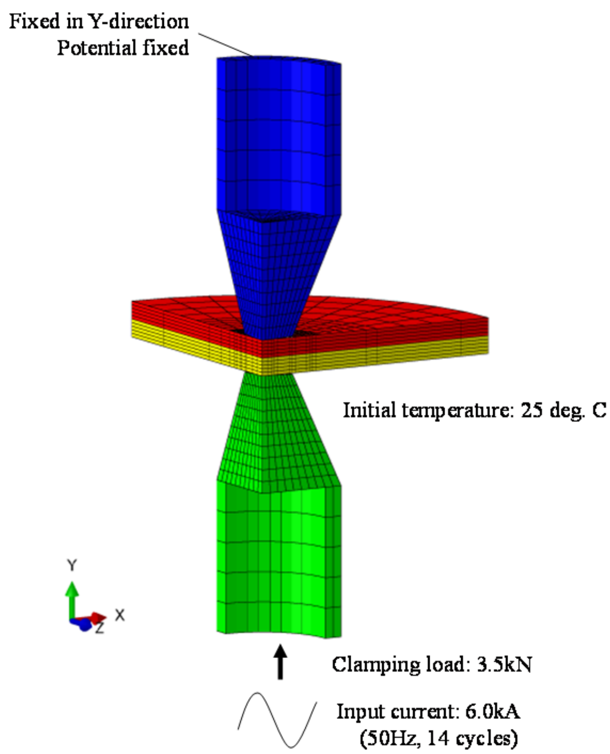

Figure 1. Analysis model.

Boundary conditions are also shown in Figure 1. In addition to the symmetry conditions, the top surface of the upper electrode is constrained in the y-direction. Reference electric potential (voltage) is also specified to the top surface. While the electrical loading is given with specified current, some reference potential is required to be defined as a boundary condition. The mechanical and electrical loading scheme is as follows.

Step 1: The initial temperature of the whole model is set at 25 °C. The clamping load of 3.5kN is applied to the bottom surface of the lower electrode (i.e., 1/4 of 3.5kN is applied to the model due to symmetry).

Step 2: While the clamping load is kept constant, the electric current of 6.0kA is applied (i.e., 1/4 of 6.0kA is applied). For avoiding excessive heating, the electric current is given as cyclic input (14 cycles at frequency of 50Hz). Joule heating is provided, and the nugget is generated.

Step 3: After completion of the electric loading, the mechanical loading is unloaded. Then, the nugget is cooled to accomplish a welded joint.

Following the above-mentioned procedure, the nugget-formation process can be analyzed quantitatively by a fully automatic and seamless simulation. It is also possible to examine residual stresses because the mechanical part of the coupled analysis is treated as an elastoplastic thermal stress field. Refer to the Appendix to unify the unit system for the coupled thermal-electrical-structural analysis.

3. Material modeling

3.1 Material modeling of steel sheet

During the cooling stage in welding processes, the phase transformation from the austenitic phase to the martensitic phase may occur. Therefore, it is necessary to consider the change in phase fraction of austenite to accurately estimate the residual stresses. However, it is rather difficult to treat the phase change for the standard Abaqus analysis, so this issue is left for a future challenge. Instead, simply assuming austenitic steel material, the analysis is carried out in this study laying emphasis on the growth process of a nugget. Figure 2 shows material constants of the steel sheet. Temperature dependency is taken into account for Young’s modulus and the yield stress of the steel sheet. The steel sheet is assumed to have a semi-molten temperature of around 1,000 °C or higher, and Young’s modulus and the yielding stress are lowered to the appropriately settled minimum value in this temperature region. Poisson’s ratio is kept constant as 0.3.

For the heat transfer analysis, thermal conductivity and specific heat are assumed to have temperature dependency as shown in Figure 3. Mass density is kept constant as 7.80E-9 ton/mm^3, and the thermal expansion coefficient is kept constant as 1.20E-5 °C^{-1}. Temperature-dependent electrical conductivity is assigned as shown in Figure 4.

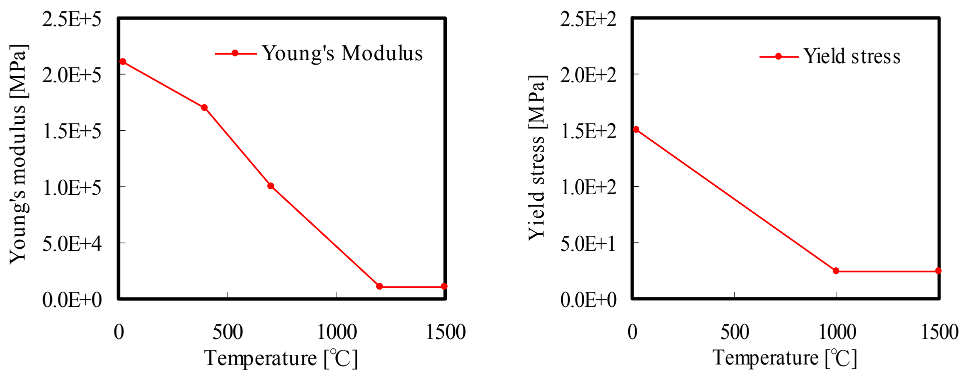

Figure 2. Mechanical properties of the steel sheet.

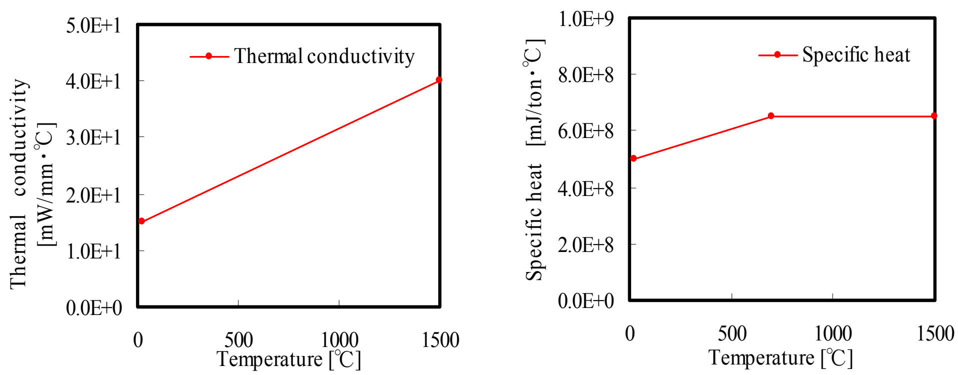

Figure 3. Thermal properties of the steel sheet.

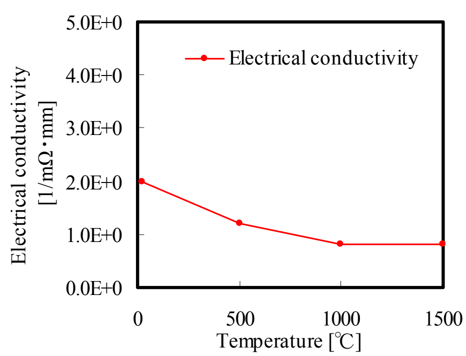

Figure 4. Electrical properties of the steel sheet.

3.2 Material modeling of the electrode

Material properties of the electrode are shown in Table 1 through Table 3. The electrode is assumed to consist of aluminum oxide dispersion-strengthened copper alloy. The material properties of the copper alloy are substantially close to pure copper. It should be noted that both the thermal conductivity and the electrical conductivity of the copper alloy are higher than those of the steel sheet by an order or more of magnitude; that is, the alloy's thermal conductivity is10 – 25 times and electrical conductivity is 30 – 70 times that of steel. As the electrical conductivity of the electrode is relatively high compared with that of the steel sheet, cooling the electrode is easily achieved even in high-power current applications. Resultantly, rising of the surface temperature of the steel sheets is suppressed, and accordingly the nugget can be limited to grow only within the sheet thickness. From the viewpoint of the electric resistance (the reciprocal of the electrical conductivity), the steel sheet has far higher resistance than the electrode. Accordingly, the Joule heat generation takes place only inside the steel sheets. That is to say, by giving the difference in conductive properties between the steel sheet and the electrode, the melting zone can be controlled to within a certain portion of the sheet, which allows the formation of the properly sized nugget.

Table 1. Mechanical properties of the electrode.

Young's Moulus	MPa	1.10E+05
Poisson's ratio	-	3.30E-01

Table 2. Thermal properties of the electrode.

Mass density	ton/mm^3	8.90E-09
Thermal conductivity	mW/mm·℃	3.60E+02
Specific heat	mJ/ton·℃	4.20E+08

Table 3. Electrical properties of the electrode.

Electrical conductivity	/mΩ·mm	5.80E+01

3.3 Properties of the sheet-to-sheet interface

Contact conditions in coupled thermal-electrical analysis can be represented using thermal contact conductance and electrical contact conductance. Because these properties may vary depending on the nature of the steel sheet surface as well as the surface contact pressure, experimental investigations are essentially required. However, in this study, which aims to search the required and/or adequate magnitude of these conductances through simulation, constant values are assumed as provided in Table 4 and Table 5. The overall heat transfer coefficient λ/t and the overall electric transfer coefficient σ/t of the steel sheet can be simply estimated as following the formula. The magnitude of the conductances shown in Table 4 and Table 5 are defined to be nearly equivalent to, or somewhat lower than, these overall transfer coefficients of the steel sheet. Note that the sheet-to-sheet thermal contact conductance may not affect the analysis results due to upper- and lower symmetry of the model.

Overall heat transfer coefficient of steel plate: $\frac{\lambda}{t} = \frac{15 \sim 40}{1.6} = 9.4 \sim 25 \quad [mW / mm^2 \cdot ℃]$

Overall electric transfer coefficient of steel plate: $\frac{\sigma}{t} = \frac{0.8 \sim 2.0}{1.6} = 0.5 \sim 1.25 \quad [1 / m\Omega \cdot mm^2]$

Table 4. Thermal contact conductance for the sheet-to-sheet interface.

Interface pressure		Thermal contact conductance	
0.00E+00	MPa	2.00E+01	$mW/mm^2 \cdot ℃$
1.00E+03		2.00E+01	

Table 5. Electrical contact conductance for the sheet-to-sheet interface.

Interface pressure		Electrical contact conductance	
0.00E+00	MPa	2.00E-01	$/m\Omega \cdot mm^2$
1.00E+03		2.00E-01	

3.4 Properties of the electrode-to-sheet interface surface

The thermal contact conductance and the electrical contact conductance for the electrode-to-sheet contact interface are shown in Table 6 and Table 7. Both of the conductances are given as high as ten times the values set for the sheet-to-sheet contact conductances in Table 4 and Table 5.

Table 6. Thermal contact conductance for the electrode-to-sheet interface.

Interface pressure		Thermal contact conductance	
0.00E+00	MPa	2.00E+02	$mW/mm^2 \cdot ℃$
1.00E+03		2.00E+02	

Table 7. Electrical contact conductance for the electrode-to-sheet interface.

Interface pressure		Electrical contact conductance	
0.00E+00	MPa	2.00E+00	$/m\Omega \cdot mm^2$
1.00E+03		2.00E+00	

Based on the above setting, the thermal contact conductances and the overall heat transfer coefficients are ordered in terms of magnitude as shown below. This allows for the effective cooling of electrodes and, consequently, suppressing the rise in temperature for the steel sheet surfaces.

- **Desired order of thermal conductance magnitude;**

  Electrode > Electrode-to-sheet > (Steel sheet ~ Sheet-to-sheet)

Setting the order of the electric resistances (the reciprocal of the electrical conductivity) as shown below makes it possible for the heat generation to be selectively initiated on the sheet-to-sheet contact interface. Similar to the previously mentioned thermal properties of the copper-alloy electrode, such ordering is advantageous for forming a properly sized nugget.

- **Desired order of electric resistance magnitude;**

  (Sheet-to-sheet ~ Steel sheet) > Electrode-to-sheet > Electrode

4. Analysis results

4.1 Nugget growth mechanism

The loading history of the clamping load and the input current are shown in Figure 5. In the initial time of 0.1 sec, the clamping load of 3.5kN is applied. In the next duration of 0.28 sec, the electric current of 6.0kA is applied with 14 cycles at a frequency of 50 Hz. In the last duration of 0.1 sec, the clamping load is unloaded. The history of the resultant potential is shown in Figure 6. The potential also periodically varies corresponding to the input current cycles. The electric resistance of the steel sheets increases along with temperature as shown in Figure 4. However, the effect from the increase in the contact area caused by softening the steel sheets exceeds this effect; hence, the potential tends to decrease.

Temperature history obtained at the center of the sheet-to-sheet interface is shown in Figure 7. The temperature sharply increases simultaneously along with the electric current loading, and thereafter, will stay at a nearly constant level after exceeding 2000 °C. Figure 8 indicates the path plots of temperature and potential on the central axis at the 14th cycle of the current loading. A large difference in potential is produced on the sheet-to-sheet interface, with which a local heat generation is provided.

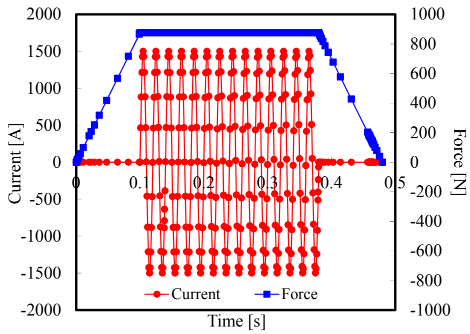

Figure 5. Clamping load and input current.

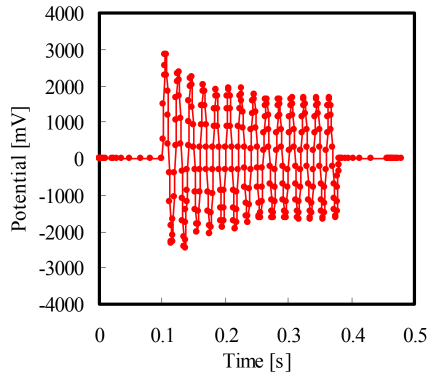

Figure 6. Resultant potential.

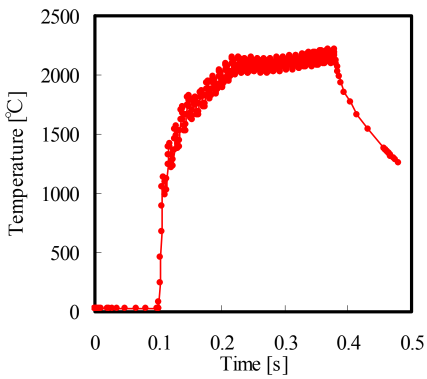

Figure 7. Temperature of sheet-to-sheet interface.

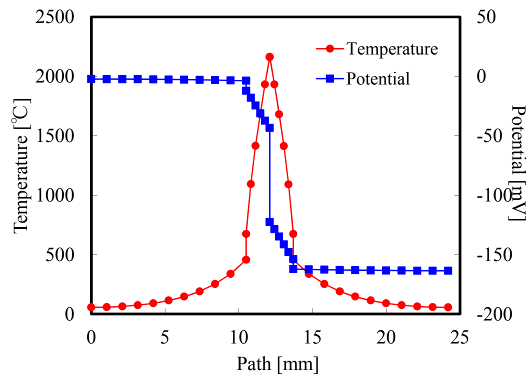

Figure 8. Joule heat generation.

Growth of the nugget diameter and the nugget penetration ratio (ratio of the nugget penetration depth to the sheet thickness) during the 1st to 14th cycles is plotted in Figure 9. Distribution of temperature and electric current density obtained at typical time steps (1, 2, 4, 8, and 14 cycle) are shown in Figure 10. The temperature zone indicated in gray was heated over 1450 °C, and the zone is assumed as melted, that is, a nugget. At the end of the 1st cycle, the nugget is not yet generated while the sheet-to-sheet interface temperature is rising. After that, the nugget extensively grows up mainly into the thickness direction of the steel sheets during the 2nd to 6th cycle. This growth progresses by concentrating the current into the narrow clamped area directly underneath the electrodes. The shaped electrode with a proper curvature is effective to make the current density concentrated during the initial stage of the welding process. During the later stage of the process, the expanding of the electrode-to-sheet contact area due to the softening of the heated steel sheets diffuses the current density. Resultantly, the nugget growth rate becomes moderate after the 7th cycle.

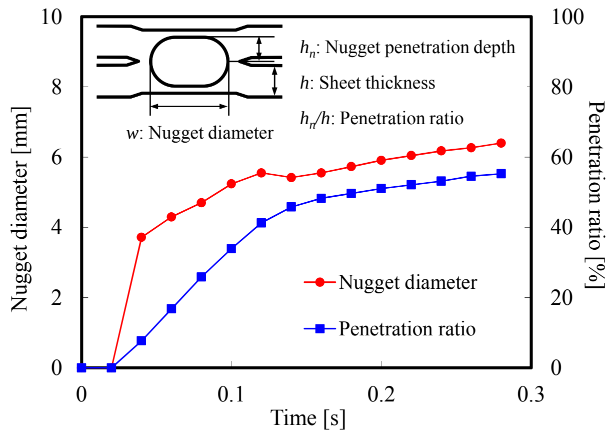

Figure 9. Predicted nugget formation process.

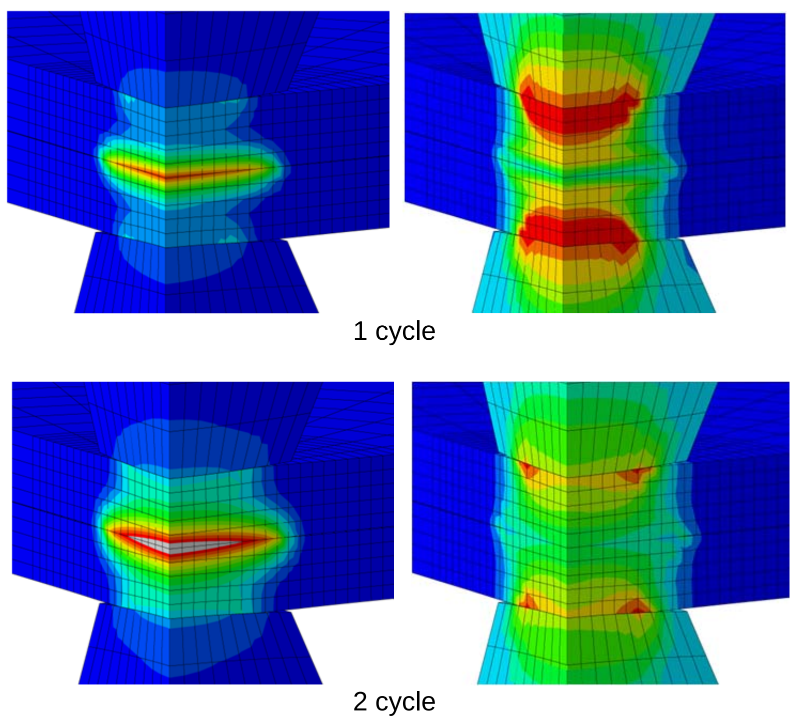

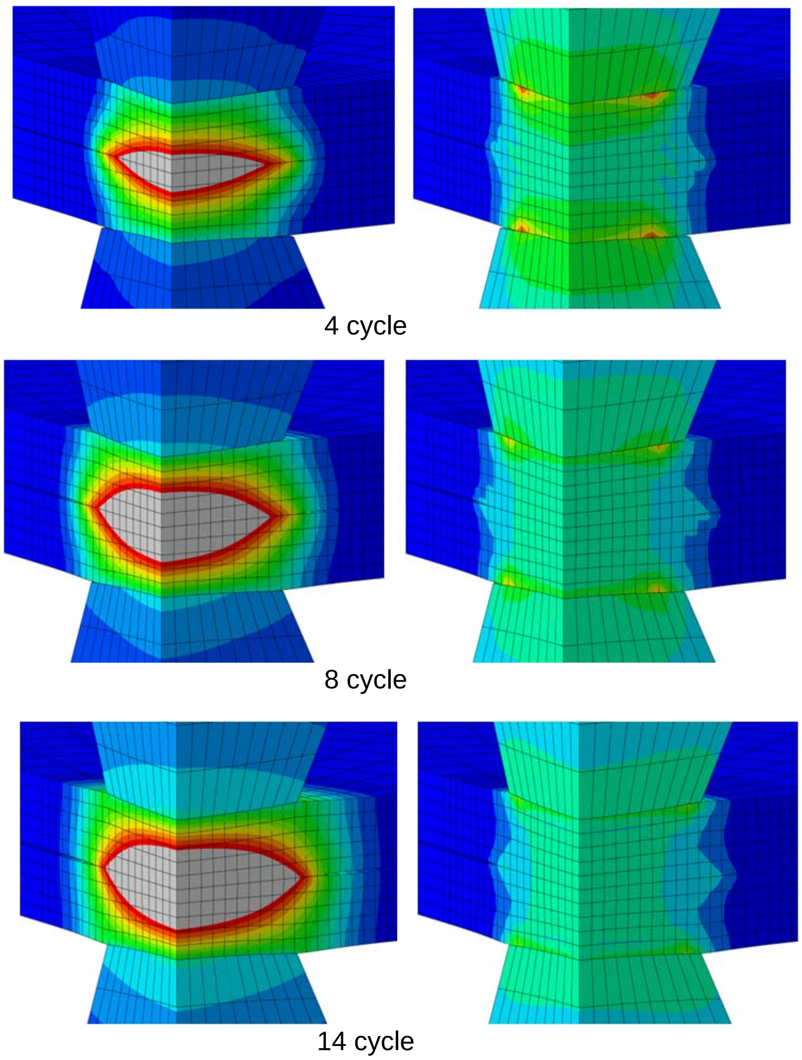

Figure 10. Nugget formation process (left: temperature; right: current density).

4.2 Effects of the clamping load

The effects of the clamping load on the nugget growth are examined in the range of loading from 1.5kN to 5.5kN. Figure 11 shows the temperature distribution after the completion of the 14th cycle for each loading case. The relationship of the nugget diameter and the penetration ratio associated with the loading magnitude is shown in Figure 12. Increasing the clamping load causes two conflicting effects: expanding the heated contact area and diffusing the current density. As a result of these trade-offs, a maximum value of the nugget diameter is given at a certain clamping load (3.5kN in Figure 12). In the same figure, the nugget penetration ratio is found to tend to reduce via an inflection point at the clamping load of 3.5kN, along with the increasing clamping load. The magnitude of the current density may be a dominant factor for the nugget penetration in the vertical direction, while the melting zone is controlled to within the sheet thickness by the cooling of the electrode.

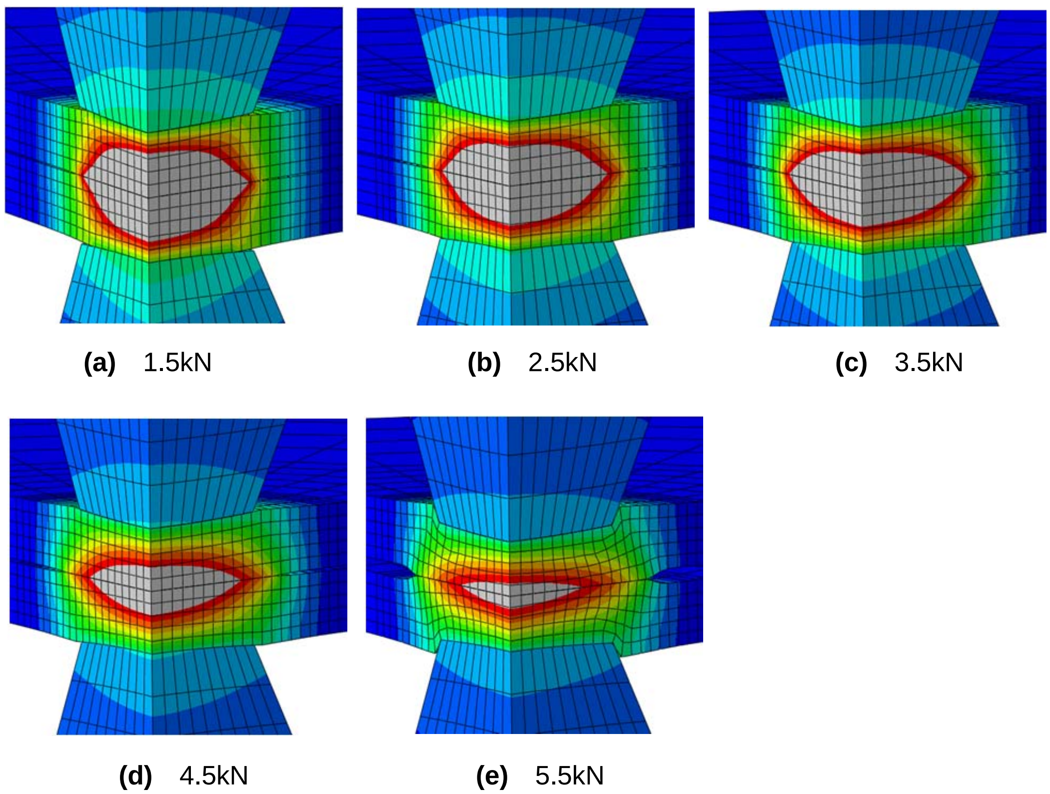

Figure 11. Effect of the clamping load on nugget formation.

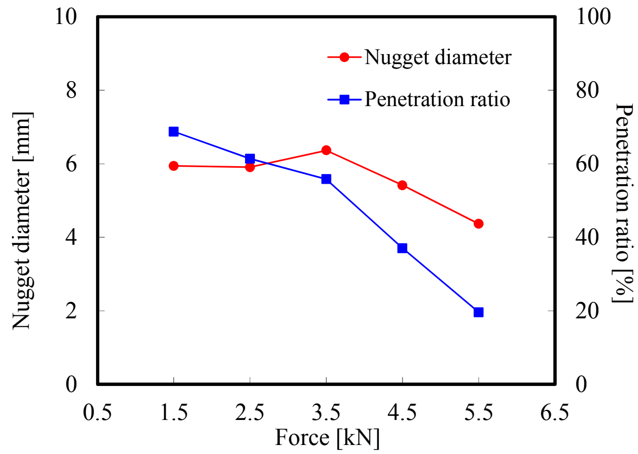

Figure 12. Effect of the clamping load on nugget formation.

4.3 Effects of the input current

The effects of the input current on the nugget growth are examined in the range of current from 5.0kA to 7.0kA. Figure 13 shows the temperature distribution after the completion of the 14th cycle for each current case. The relationship of the nugget diameter and the penetration ratio associated with the input current is shown in Figure 14. Increase of the input current provides monotonic increasing of both the nugget diameter and the penetration ratio. However, softening of the steel sheet causes the expansion of the contact area and the reduction of the current density. Therefore, the increase of the nugget size is saturated in the region of the input current of more than 6kA. It should be noted that the powerful and detailed capability of Abaqus makes it possible to realize a direct examination of the coupled phenomena, including all nonlinearities: material nonlinearity, geometrical nonlinearity, and boundary condition nonlinearity.

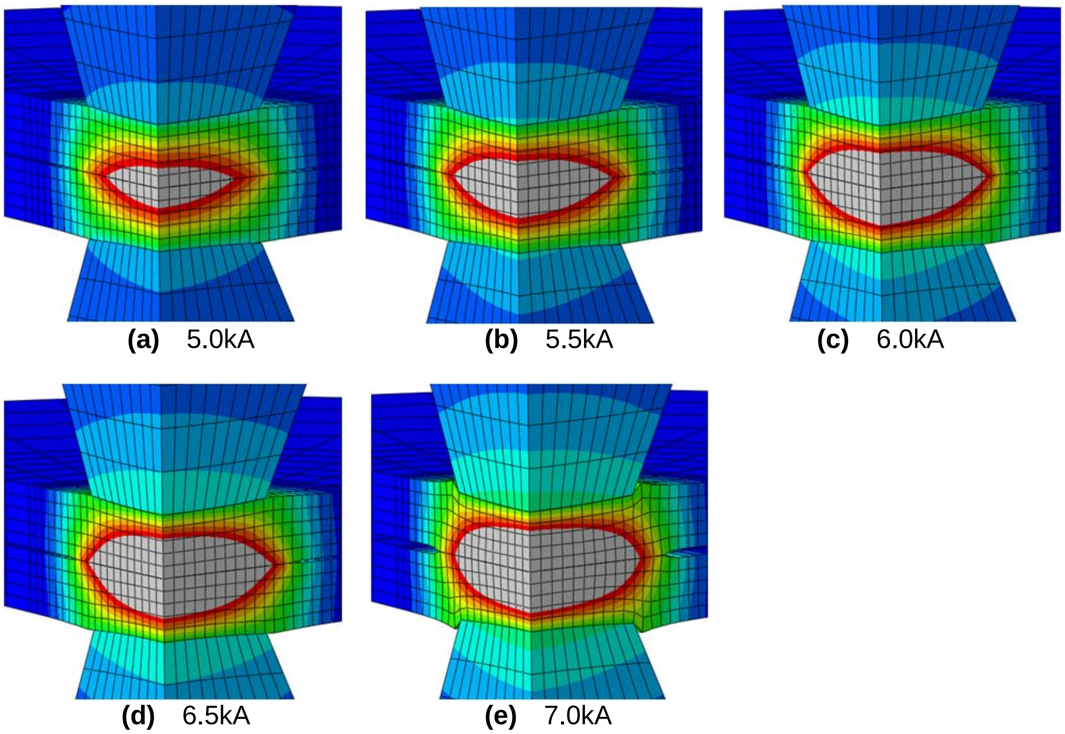

Figure .13 Effect of the input current on nugget formation.

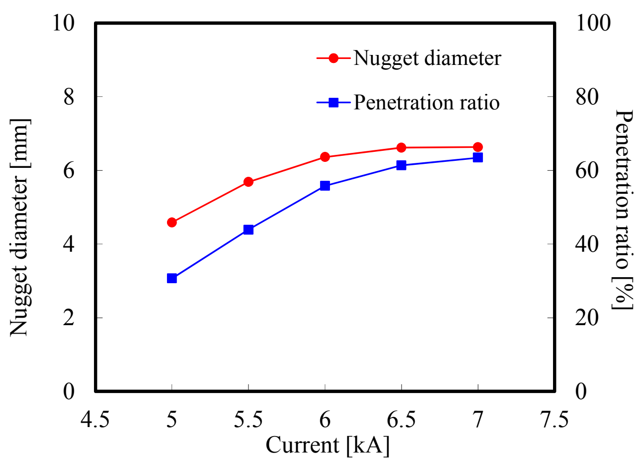

Figure .14 Effect of the input current on nugget formation.

4.4 Residual stress

Figure 15 shows the post-cooling residual stress pattern. Existence of tensile residual stress near the outer circumference of the nugget is recognized. For steel alloys, the two phases are normally termed as the austenitic (stable at higher temperatures) and martensitic phase (stable at lower temperatures). When the steel is in an austenitic phase and then quenched rapidly, it forms into martensite, which has a lower density and a higher strength than austenite. Therefore, for more accurate estimation of residual stress, it is necessary to consider the phase fraction.

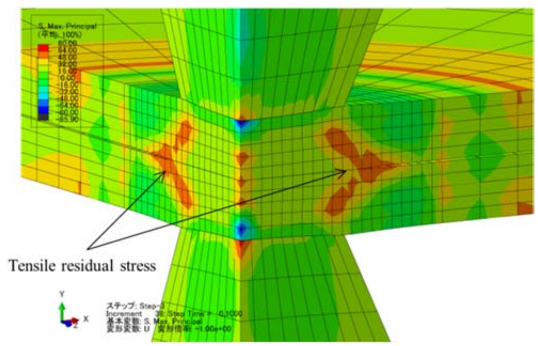

Figure 15. Resultant residual stress.

5. Conclusion

Using the coupled thermal-electrical-structural analysis capability recently implemented into Abaqus, numerical simulations of the spot welding was carried out. In this study, with particular interest in the interface surface properties, a quantitative estimation was performed for the nugget growth process. Although the accurate estimation of residual stress remaining after the cooling stage is a great problem, it will be a future task.

6. Appendix: Notes for the unit system

This study is regarded as a typical example of multi-physics. For prompting fundamental understanding, the explanations for the unit system applied in this study are shown below.

For the base units of stress analysis, length: mm, mass: ton, and time: s are employed. Accordingly, derived units of force: ton・mm/s^2 = 10^{3}kg・10^{-3}m/s^2 = N, and stress: N/mm^2 = Mpa are given.

Considering thermal-electrical-structural coupling, the common physical quantity is energy (work), which is defined as follows: Energy: N・mm = N・10^{-3}m = mJ (millijoule). Accordingly, derived thermal units, mass density: ton/mm^3, thermal conductivity: mW/mm・℃ (milliwatt/mm・℃), and specific heat: mJ/ton・℃ (millijoule/ton・℃) are defined.

For electrical units, electric current: A is employed as the base unit. With caution in order to make energy units consistent, potential (=electric power/electric current): mW/A=mV (millivolt), and electric resistance (=potential/electric current): mV/A=mΩ (milliohm) are defined.

7. References

1. *Abaqus Users Manual*, Version 6.11, Dassault Systems Simulia Corp., USA, 2011.
2. M. Iyota, Y. Mikami, T. Hashimoto, K. Taniguchi, R. Ikeda and M. Mochizuki, Effect of electrode force condition on nugget diameter and residual stress in resistance spot welded high-strength steel sheets, Journal of Physics: Conference Series 379, 2012.
3. M. Iyota, Y. Mikami, T. Hashimoto, K. Taniguchi, R. Ikeda and M. Mochizuki, Numerical Simulation of Nugget Size and Residual Stress of Resistance Spot Welded HT980 Steel Sheet (in Japanese), *Quarterly Journal of the JWS,* Vol. 29, No. 2, pp. 86–95, 2011.
4. J. A. Khan, L. Xu, Y. Chao, K. Broach, Numerical Simulation of Resistance Spot Welding Process, Numerical Heat Transfer, Part A: Applications, *An International Journal of Computation and Methodology,* Vol. 37-5, pp. 425–446, 2000.
5. E. Feulvarchab, P. Rogeonc, P. Carréc, V. Robinb, G. Sibiliad and J. M. Bergheaua, Resistance Spot Welding Process: Experimental and Numerical Modeling of the Weld Growth Mechanisms with Consideration of Contact Conditions, Numerical Heat Transfer, Part A: Applications, *An International Journal of Computation and Methodology,* Vol. 49-4, pp. 345–367, 2006.